JOURNAL OF SOLID STATE CHEMISTRY 78, 7–16 (1989)

Synthesis, Structures, and Conductivities of the New Layered Compounds $Ta_3Pd_3Te_{14}$ and $TaNiTe_5$

ERIC W. LIIMATTA AND JAMES A. IBERS*

Department of Chemistry, Northwestern University, Evanston, Illinois 60208

Received March 31, 1988; in revised form May 31, 1988

The new layered ternary chalcogenides $Ta_3Pd_3Te_{14}$ and $TaNiTe_5$ have been prepared by high-temperature reactions of the elements. They have been characterized by single crystal X-ray diffraction methods. The compound $Ta_3Pd_3Te_{14}$ crystallizes with two formula units in the monoclinic space group C_{2h}^2–$P2_1/m$ in a cell with dimensions $a = 14.088(19)$, $b = 3.737(3)$, $c = 20.560(19)$ Å, and $\beta = 103.73(5)°$. $TaNiTe_5$ crystallizes with four formula units in the orthorhombic space group D_{2h}^{17}–$Cmcm$ in a cell with dimensions $a = 3.659(2)$, $b = 13.122(10)$, $c = 15.111(11)$ Å. Both are layer structures. $TaNiTe_5$ is isostructural with the previously synthesized compound $NbNiTe_5$. The layers for $TaNiTe_5$ contain Ta atoms in a bicapped trigonal prismatic Te environment and Ni atoms in an octahedral environment. The layers for $Ta_3Pd_3Te_{14}$ are made up of octahedral and bicapped trigonal prismatic Ta atoms and octahedral Pd atoms coordinated by Te. Electrical conductivity measurements indicate that both of these compounds are metallic; for $Ta_3Pd_3Te_{14}$, $\sigma_{297} \approx 2.2 \times 10^3\ \Omega^{-1}\ cm^{-1}$ and for $TaNiTe_5$, $\sigma_{297} \approx 2.6 \times 10^4\ \Omega^{-1}\ cm^{-1}$. Magnetic susceptibility measurements show that $TaNiTe_5$ is paramagnetic.

Introduction

Even though there has been an enormous interest in the Group V binary and ternary chalcogenides because of their structural and physical properties (*1–6*), the chemistry of the Group V tellurides is still relatively unexplored. Aside from the intercalation compounds Huan and Greenblatt (*7, 8*) recently reported only five ternary niobium tellurides ($Sb_2Nb_3Te_5$ (*9*), Cu_3NbTe_4 (*10*), Ag_2NbTe_3 (*11*), $NbNiTe_5$ (*12*), $NbPdTe_5$ (*13*)) and three ternary Ta tellurides (Cu_3TaTe_4 (*10*), Ag_2TaTe_3 (*11*), Mo_2TaTe_4 (*14*)) have been reported in the literature.

As an extension of our interest in the system $M/M'/Q$ (*15–26*), where M = Nb or Ta, M' = Ni, Pd, or Pt, and Q = S or Se, we began investigations of telluride compounds in this system. We showed in our earlier work that in certain cases S can substitute for Se (*17, 19*) with very little effect on the structural or physical properties. If one extrapolates this behavior to Te, one might expect new tellurides to be isostructural with existing sulfides and selenides. Indeed, Cu_3NbS_4, Cu_3NbSe_4, and Cu_3NbTe_4 are isostructural (*10*). However, we recently reported the synthesis and characterization (*12*) of the first layered ternary telluride $NbNiTe_5$. $NbNiTe_5$ has a different stoichiometry, has a unique structural type, and has different physical

* To whom all correspondence should be addressed.

0022-4596/89 $3.00

properties from any sulfide or selenide synthesized previously in this laboratory. Here we report the synthesis and characterization of the isostructural compound $TaNiTe_5$ as well as the synthesis and characterization of the new layered telluride $Ta_3Pd_3Te_{14}$ that resulted from our attempt to synthesize the unknown compound $TaPdTe_5$.

Experimental

Synthesis. The compound $Ta_3Pd_3Te_{14}$ was prepared from the powders of the elements (Ta, 99.98%, Aesar; Pd, 99.95%, Alfa; Te, 99.99%, Aesar). These were loaded in a silica tube in the atomic ratio Ta : Pd : Te = 3 : 1 : 8. A large amount of I_2 (≈20% by wt.) was added as a transport agent and appears to be necessary for crystal growth. The portion of the silica tube that contained the metal powders and I_2 was submerged in liquid N_2 and then the tube was evacuated to $\approx 10^{-5}$ Torr and sealed. The tube was then heated for 8 days under a temperature gradient of 675°C on the charge end to 725°C on the transport end. Some thin gray-black needle-like crystals formed in the charge end. Analysis of these crystals with the microprobe of an EDAX equipped Hitachi S570 scanning electron microscope showed only the presence of Ta, Pd, and Te.

The compound $TaNiTe_5$ was also prepared from the powders of the elements (Ni, 99.9%, Alfa). These were loaded in a silica tube in the atomic ratio Ta : Ni : Te = 3 : 1 : 8. Approximately 10% by weight of I_2 was added as a transport agent. Iodine is essential for crystal growth. The part of the silica tube that contained the metal powders and I_2 was submerged in liquid N_2 and then the tube was evacuated to $\approx 10^{-5}$ Torr and sealed. The tube was then heated for 8 days under a temperature gradient of 700°C on the charge end to 750°C on the transport end. Some thin gray-black needle-like crystals formed in the charge end. Analysis of these crystals by EDAX showed only the presence of Ta, Ni, and Te. Quantitative analysis was performed on four crystals with the use of the program MICROQ (*27*). Crystals of $Ta_3Pd_3Te_{14}$ and $NbNiTe_5$ were used as standards for this analysis. The analysis gave Ta 19.26(70), Ni 6.65(40), Te 74.06(72). Calculated for $TaNiTe_5$: Ta, 20.61; Ni, 6.68; Te, 72.69. These results are slightly outside the claimed accuracy for the program MICROQ of ±1 wt%. Nevertheless, these results confirm the composition of the compound.

On the basis of the EDAX measurements we estimate that if iodine is present in these materials it is there at less than 1 wt%. No structural evidence was found for the presence of iodine.

Physical properties. Four-probe ac conductivity measurements along the needle axis a of $TaNiTe_5$ and along the needle axis b of $Ta_3Pd_3Te_{14}$ were performed by procedures described previously (*28*). Magnetic susceptibility measurements were performed at 5 kG over the temperature range 2.50–200 K with a VTS-50 SQUID susceptometer (S.H.E. Co.). Sample holders made of high-purity Spectrosil quartz were used in the susceptibility measurements.

Structure determinations. Crystals of $Ta_3Pd_3Te_{14}$ exhibited monoclinic symmetry on Weissenberg photographs. The systematic extinction ($0k0$, $k = 2n + 1$) is consistent with the space group $P2_1/m$ or $P2_1$. Since the crystals were mosaic and gave broad peaks, the final lattice parameters were determined from eight hand-centered reflections in the range $14° \leq 2\theta(\text{Mo}K\alpha_1) < 21°$. Diffraction data were collected at −150°C on a Picker FACS-1 diffractometer. Table I gives details of the data collection. The data for $Ta_3Pd_3Te_{14}$ were processed and corrected for absorption effects. The centrosymmetric space group $P2_1/m$ was chosen since a satisfactory residual of 0.06 results after averaging the inner sphere (<50° in 2θ) data with $F_o^2 > 3\sigma(F_o^2)$ in $2/m$

TABLE I

CRYSTAL DATA FOR $Ta_3Pd_3Te_{14}$ AND $TaNiTe_5$

	$Ta_3Pd_3Te_{14}$	$TaNiTe_5$
Formula mass (amu)	2648.44	877.66
Space group	C_{2h}^2–$P2_1/m$	D_{2h}^{17}–$Cmcm$
a (Å)	14.088(19)	3.659(2)
b (Å)	3.737(3)	13.122(10)
c (Å)	20.560(19)	15.111(11)
β (deg)	103.73(5)	
V (Å^3)	1051.5	725.4
Z	2	4
T of data collection (K)[a]	123	123
Density (calc) (g cm^{-3})	8.13	8.03
Radiation	Graphite monochromated Mo$K\alpha_1$ ($\lambda(K\alpha_1)$ = 0.7093 Å)	
Crystal shape	Flattened rod bounded by {010} {$\bar{1}$01} {301}	Flattened rod bounded by {100} {010} {001} (0$\bar{2}$1)
Crystal vol. (mm^3)	2.47×10^{-4}	2.7×10^{-4}
Linear abs. coeff. (cm^{-1})	358.9	371.7
Transmission factors[b]	0.345–0.696	0.261–0.476
Detector aperture (mm)	horizontal, 6.0 vertical, 6.0 32 cm from crystal	horizontal, 4.5 vertical, 4.0 32 cm from crystal
Takeoff angle (deg)	2.5	2.5
Scan type	ω	θ–2θ
Scan speed (deg min^{-1})	1.0 in ω	2.0 in 2θ
Scan range	−1.0 to +1.0°	1.0° below $K\alpha_1$ to 0.8° above $K\alpha_2$
2θ limits (deg)	$3 < 2\theta < 51$ $56 < 2\theta < 59.5$[c]	$3 \leq 2\theta \leq 73$
Background counts[d]	10 sec at each end of scan	10 sec at each end of scan
Data collected	$\pm h \pm k \pm l$	$\pm h \pm k \pm l$
p factor	0.04	0.04
No. of data collected	11,901	7,132
No. of unique data	2,837	1,039
No. of unique data with $F_o^2 > 3\sigma(F_o^2)$	1,473	964
No. of variables	121	25
$R(F^2)$	0.106	0.074
$R_w(F^2)$	0.126	0.084
R (on F for $F_o^2 > 3\sigma(F_o^2)$)	0.052	0.034
Error in observation of unit weight (e^2)	1.18	1.58

[a] The low-temperature system is based on a design by Huffman (*43*).

[b] An analytical absorption correction was applied with the use of the method of de Meulenaer and Tompa (*44*).

[c] The data from 46 to 51° were collected twice and the data from 51 to 56° were inadvertently not collected.

[d] The diffractometer was operated under the Vanderbilt disk orientated system (*45*). The data collection for $TaNiTe_5$ used a rescan option while the data collection for $Ta_3Pd_3Te_{14}$ did not use a rescan option.

symmetry. The initial positions for all the atoms in $Ta_3Pd_3Te_{14}$ were found with the program SHELXS-86 (*29*). All subsequent calculations for $Ta_3Pd_3Te_{14}$ and all calculations for $TaNiTe_5$ were carried out with methods standard for this laboratory (*30–32*). The final cycle of refinement on F_o^2 included anisotropic thermal parameters and resulted in a value of $R(F_o^2)$ of 0.106. The function minimized was $\Sigma w(F_o^2 - F_c^2)^2$. The value for the conventional R index (on F for $F_o^2 > 3\sigma(F_o^2)$) is 0.052. The satisfactory refinement justifies the choice of the centrosymmetric space group $P2_1/m$. The final difference electron density map showed no peak higher than 5.0% the height of a Ta atom.

Preliminary lattice parameters and the orthorhombic symmetry of $TaNiTe_5$ were determined from Weissenberg photographs. The final lattice parameters were determined from least-squares analysis of the setting angles of 15 reflections in the range $22° \leq 2\theta(MoK\alpha_1) < 28°$ automatically centered on a Picker FACS-1 diffractometer. Diffraction data were collected at −150°C. Table I gives details of the data collection. The data were processed and corrected for absorption effects. The centrosymmetric space group *Cmcm* was chosen since a satisfactory residual of 0.03 results after averaging the inner sphere of data ($2\theta < 50°$; $F_o^2 > 3\sigma(F_o^2)$) in *mmm* symmetry. The initial positions for the atoms in $TaNiTe_5$ were taken from the atomic positions of the isostructural compound $NbNiTe_5$. This led to a satisfactory least-squares refinement. The final cycle of refinement on F_o^2 included anisotropic thermal parameters and resulted in a value of $R(F_o^2)$ of 0.074. The value for the conventional R index (on F for $F_o^2 > 3\sigma(F_o^2)$) is 0.034. The final difference electron density map showed no peak higher than 1.4% the height of a Ta atom.

The refined values of the thermal parameters for both $Ta_3Pd_3Te_{14}$ and $TaNiTe_5$ are consistent with stoichiometric structures. No unusual trends were found in an analysis of F_o^2 versus F_c^2 as a function of F_o^2, setting angles, and Miller indices for $Ta_3Pd_3Te_{14}$ and $TaNiTe_5$. Final values of the atomic parameters for $Ta_3Pd_3Te_{14}$ and $TaNiTe_5$ are in Table II. Final anisotropic thermal parameters and structure amplitudes for both structures are given in Tables III[1] and IV.[1]

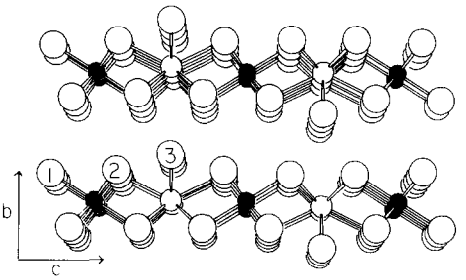

FIG. 1. View of $TaNiTe_5$ down the *a* axis, showing the labeling scheme. Here and in Fig. 2 small filled circles are Ni, small open circles are Ta, and large open circles are Te atoms.

Results. Selected bond distances and angles for $TaNiTe_5$ are given in Table V. A drawing of the structure is given in Fig. 1. The structure consists of bicapped trigonal prismatic Ta atoms and octahedral Ni atoms that lie in two chains running parallel to the *c* axis. Figure 2 shows the coordination around the Ta and Ni atoms. A detailed description of the $NbNiTe_5$ structural type has been given previously (*12*). The bond distances and angles in $TaNiTe_5$ and the isostructural compound $NbNiTe_5$ are very similar. This is not surprising given the very similar sizes of Nb and Ta in comparable oxidation states (*33*).

The electrical conductivity of $TaNiTe_5$ measured along the *a* axis from 14 to 297 K

[1] See NAPS Document No. 04608 for 19 pages of supplementary materials from ASIS/NAPS, Microfiche Publications, P.O. Box 3513, Grand Central Station, New York, NY 10163. Remit in advance $4.00 for microfiche copy or for photocopy, $7.75. All orders must be prepaid.

TABLE II

POSITIONAL PARAMETERS AND B_{eq} FOR $TaNiTe_5$ AND $Ta_3Pd_3Te_{14}$

Atom	Wyckoff notation	x	y	z	B_{eq} (Å^2)
			$TaNiTe_5$		
Te(1)	8f	0	0.100965(36)	0.144687(32)	0.378(9)
Te(2)	8f	$\frac{1}{2}$	0.107814(36)	0.575017(32)	0.42(1)
Te(3)	4c	0	0.174901(52)	$\frac{3}{4}$	0.40(1)
Ta	4c	$\frac{1}{2}$	−0.012949(31)	$\frac{1}{4}$	0.287(8)
Ni	4a	0	0	0	0.42(2)
			$Ta_3Pd_3Te_{14}$		
Ta(1)	2e	0.30008(11)	$\frac{1}{4}$	0.544125(73)	0.62(4)
Ta(2)	2e	0.94616(11)	$\frac{1}{4}$	0.189372(74)	0.59(3)
Ta(3)	2e	0.57652(11)	$\frac{1}{4}$	0.8440981(74)	0.70(4)
Pd(1)	2e	0.74854(21)	$\frac{3}{4}$	0.01882(14)	0.67(7)
Pd(2)	2e	0.12900(23)	$\frac{3}{4}$	0.36518(14)	0.81(6)
Pd(3)	2e	0.48160(21)	$\frac{3}{4}$	0.72644(14)	0.82(7)
Te(1)	2e	0.31546(18)	$\frac{3}{4}$	0.44318(11)	0.74(6)
Te(2)	2e	0.14463(18)	$\frac{1}{4}$	0.27515(12)	0.80(6)
Te(3)	2e	0.60799(19)	$\frac{1}{4}$	0.98927(12)	0.82(6)
Te(4)	2e	0.72813(17)	$\frac{3}{4}$	0.88573(11)	0.67(6)
Te(5)	2e	0.45413(18)	$\frac{3}{4}$	0.58648(12)	0.65(6)
Te(6)	2e	0.18099(17)	$\frac{3}{4}$	0.59195(12)	0.74(6)
Te(7)	2e	0.88925(18)	$\frac{1}{4}$	0.04458(12)	0.68(5)
Te(8)	2e	0.78961(17)	$\frac{3}{4}$	0.15397(12)	0.73(6)
Te(9)	2e	0.33894(18)	$\frac{1}{4}$	0.68864(12)	0.82(6)
Te(10)	2e	0.94291(18)	$\frac{3}{4}$	0.29302(11)	0.67(6)
Te(11)	2e	0.62294(18)	$\frac{1}{4}$	0.72768(12)	0.78(6)
Te(12)	2e	0.05941(17)	$\frac{3}{4}$	0.13691(11)	0.70(6)
Te(13)	2e	0.43535(17)	$\frac{3}{4}$	0.84930(12)	0.71(5)
Te(14)	2e	0.10622(18)	$\frac{1}{4}$	0.45371(12)	0.78(6)

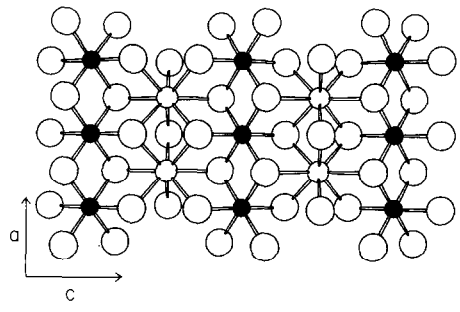

FIG. 2. View of $TaNiTe_5$ down the b axis showing the coordination around the Ta and Ni atoms.

TABLE V

SELECTED INTERATOMIC DISTANCES (Å) AND ANGLES (DEG) FOR $TaNiTe_5$

Ta–2Te(3)	2.804(2)	Te(1)–Ni–4Te(2)	95.26(4)
Ta–4Te(1)	2.848(1)	Te(2)–Ni–2Te(2)	90.52(5)
Ta–2Te(2)	2.923(2)	Te(3)–Ta–Te(3)	81.44(6)
Ta–2Ta	3.659(2)	Te(3)–Ta–4Te(2)	71.16(2)
Ta–4Ni	4.201(3)	Te(3)–Ta–4Te(1)	88.78(5)
Ni–2Te(1)	2.557(2)	Te(2)–Ta–Te(2)	129.58(5)
Ni–4Te(2)	2.575(1)	Te(1)–Ta–4Te(2)	73.62(4)
Ni–2Ni	3.659(2)	Te(1)–Ta–2Te(1)	67.93(5)
Te(1)–Te(1)	3.183(3)	Te(1)–Ta–2Te(1)	79.91(5)
Te(1)–2Te(2)	3.458(2)		
Te(1)–2Te(1)	3.659(2)		
Te(1)–2Te(2)	3.791(2)		
Te(1)–4Te(3)	3.812(2)		
Te(2)–4Te(3)	3.334(2)		
Te(2)–Te(2)	3.626(2)		
Te(2)–2Te(2)	3.659(2)		
Te(3)–2Te(3)	3.659(2)		

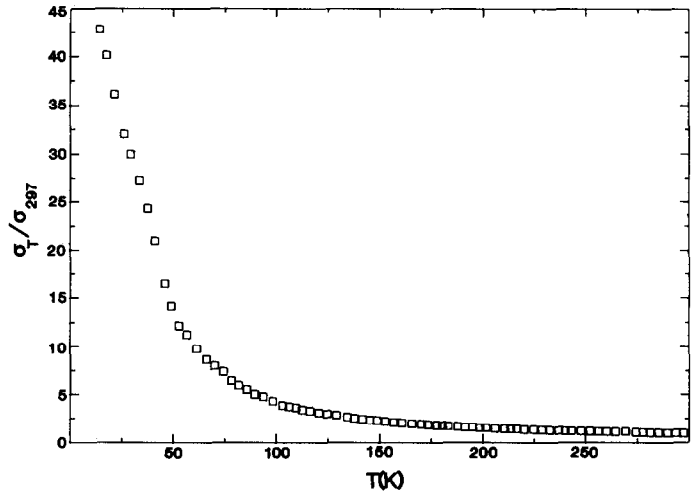

FIG. 3. Normalized plot of conductivity vs temperature along a for $TaNiTe_5$: $\sigma_{297} \approx 2.6 \times 10^4\ \Omega^{-1}\ cm^{-1}$, $\sigma_{14} \approx 1 \times 10^6\ \Omega^{-1}\ cm^{-1}$.

is shown in Fig. 3. $TaNiTe_5$ is a very highly conductive metal ($\sigma_{297} \approx 2.6 \times 10^4\ \Omega^{-1}\ cm^{-1}$); it exhibits conductivity behavior very similar to that of the isostructural compound $NbNiTe_5$.

Plots of the magnetic susceptibility (χ) at 5 kG field and χ^{-1} as a function of temperature for $TaNiTe_5$ are given in Fig. 4. $TaNiTe_5$ obeys the Curie–Weiss law over the temperature range 2.5–200 K. The magnetic data were corrected for ion-core diamagnetism (*34*) and then fit by a least-squares procedure to the equation $\chi = \chi_0 + (C/(T + \theta))$. Two data points near 25 K where the sample holder and sample are equal in magnitude but opposite in sign were omitted from the analysis. The values obtained for θ, C, and χ_0 are 2.97(8) K, 0.132(2) emu K $mole^{-1}$, and 1.2(5) $\times 10^{-4}$ emu $mole^{-1}$, respectively. From the for-

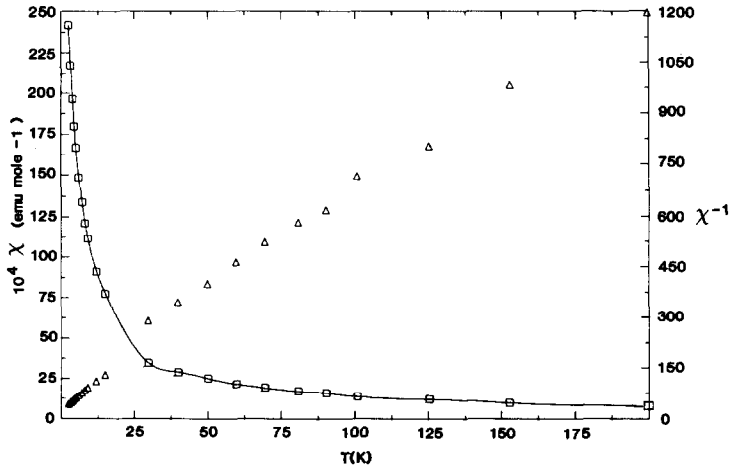

FIG. 4. Plot of χ (□) and χ^{-1} (△) as a function of temperature at 5 kG for $TaNiTe_5$.

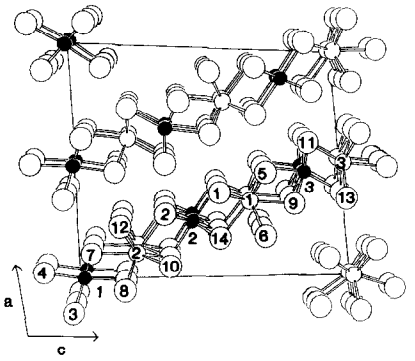

FIG. 5. View of the structure of $Ta_3Pd_3Te_{14}$ showing the labeling scheme. Here and in Fig. 5 small solid circles are Pd, small open circles are Ta, and large open circles are Te atoms.

mula (*35*) $\mu_{eff} = (8C)^{1/2}$ we obtain $\mu_{eff} = 1.03(1)\ \mu_B$. From the spin-only approximation ($\mu_{eff} = (4S(S+1))^{1/2}\ \mu_B$) the values for μ_{eff} for Ni^{2+} and Ta^{4+} are 2.83 and 1.73 μ_B, respectively, while for Ta^{5+} and Ni^0 they are 0 μ_B. Thus there must be some electron transfer from Te^{2-} to Ta^{5+} and Ni^0 to account for the measured value of μ_{eff}. This is consistent with the presence of Te–Te interactions.

Selected bond distances and angles for $Ta_3Pd_3Te_{14}$ are given in Table VI. $Ta_3Pd_3Te_{14}$ crystallizes in a new structural type. Figure 5 shows the layered nature of the structure. The structure consists of six unique chains that run parallel to the *c* axis. As one travels along *c* the composition of the chains alternates between Ta- and Pd-centered polyhedra. Figure 6 shows the coordination around the Ta and Pd atoms. The Ta atoms are in two kinds of chains: Ta-centered bicapped trigonal prisms that share triangular faces and asymmetrically Ta-centered octahedra that share edges.

The Ta–Te distances in the trigonal prism range from 2.838(3) to 2.930(5) Å. The Ta–Te distances in the octahedron range from 2.644(4) to 2.894(4) Å with the shortest distance being to an apical Te atom. This compares well with the Ta–Te distances of 2.663(8) to 2.923(7) Å found in $TaTe_2$ (*36*). The Pd atoms have octahedral coordination. The Pd–Te distances range from 2.683(5) to 2.811(5) Å. This can be compared with the Pd–Te distance found in the $Cd(OH)_2$-type $PdTe_2$ of 2.652(13) Å (*37*). There is one relatively short metal–metal interaction in this structure, a Ta–Pd distance of 3.110(3) Å. The Pd and Ta atoms shift from the center of the Te octahedra toward one another to create this short interaction. The next shortest interactions are Ta–Ta or Pd–Pd at a distance of 3.737(3) Å (the *b* repeat). The majority of the Te–Te distances in this structure range from 3.12 to 3.8 Å. These distances are significantly longer than that expected for a full Te–Te bond (2.92 Å) (*38*). These distances are also significantly shorter than twice the ionic radius of Te^{2-} (4.4 Å) (*33*). Hence, intermediate interactions are present in $Ta_3Pd_3Te_{14}$. This type of Te interaction has also been seen in $NbNiTe_5$ (*12*), $TaNiTe_5$, and $NbPdTe_5$ (*13*) and appears to be common in the Group V tellurides. This bonding behavior is probably the reason why the tellurides form compounds distinct from the sulfides and selenides, as intermediate interactions are uncommon in the latter systems.

Four-probe single-crystal conductivity measurements along the needle axis *b* show that $Ta_3Pd_3Te_{14}$ is metallic with a room-temperature conductivity of $\approx 2.2 \times 10^3\ \Omega^{-1}\ cm^{-1}$. A plot of the electrical conductivity

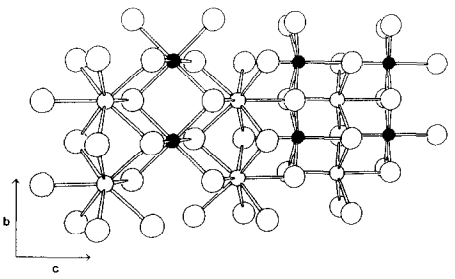

FIG. 6. Drawing of an individual layer of $Ta_3Pd_3Te_{14}$ showing the coordination around the Ta and Pd atoms.

TABLE VI

SELECTED INTERATOMIC DISTANCES (Å) AND ANGLES (DEG) FOR $Ta_3Pd_3Te_{14}$

Ta(1)–2Te(6)	2.838(3)	Te(6)–2Te(9)	3.209(4)
Ta(1)–2Te(1)	2.839(3)	Te(6)–2Te(14)	3.355(4)
Ta(1)–2Te(5)	2.839(3)	Te(7)–2Te(12)	3.268(4)
Ta(1)–Te(9)	2.890(4)	Te(7)–2Te(8)	3.467(4)
Ta(1)–Te(14)	2.916(5)	Te(8)–Te(10)	3.147(4)
Ta(2)–2Te(12)	2.832(3)	Te(8)–2Te(13)	3.666(5)
Ta(2)–2Te(10)	2.843(3)	Te(3)–Pd(1)–2Te(4)	82.8(1)
Ta(2)–2Te(8)	2.850(3)	Te(3)–Pd(1)–2Te(8)	101.5(1)
Ta(2)–Te(7)	2.893(4)	Te(7)–Pd(1)–2Te(3)	91.7(1)
Ta(2)–Te(2)	2.930(5)	Te(4)–Pd(1)–2Te(7)	95.5(1)
Ta(3)–Te(11)	2.644(4)	Te(4)–Pd(1)–Te(8)	174.0(1)
Ta(3)–2Te(13)	2.745(3)	Te(7)–Pd(1)–2Te(8)	80.2(1)
Ta(3)–2Te(4)	2.812(3)	Te(1)–Pd(2)–Te(14)	81.7(1)
Ta(3)–Te(3)	2.894(4)	Te(2)–Pd(2)–2Te(14)	91.47(9)
Ta(3)–2Pd(3)	3.110(3)	Te(10)–Pd(2)–2Te(14)	96.7(1)
Pd(1)–Te(4)	2.683(5)	Te(2)–Pd(2)–2Te(10)	81.2(1)
Pd(1)–2Te(7)	2.684(4)	Te(2)–Pd(2)–2Te(1)	100.4(1)
Pd(1)–2Te(3)	2.685(4)	Te(1)–Pd(2)–2Te(10)	177.7(1)
Pd(1)–Te(8)	2.700(5)	Te(1)–Pd(2)–2Te(14)	81.7(1)
Pd(2)–2Te(2)	2.676(3)	Te(9)–Pd(3)–2Te(13)	86.7(1)
Pd(2)–2Te(14)	2.681(3)	Te(9)–Pd(3)–2Te(5)	78.14(9)
Pd(2)–Te(10)	2.688(5)	Te(9)–Pd(3)–2Te(11)	91.2(1)
Pd(2)–Te(1)	2.734(5)	Te(11)–Pd(3)–2Te(5)	86.1(1)
Pd(3)–2Te(9)	2.719(4)	Te(11)–Pd(3)–2Te(13)	108.8(1)
Pd(3)–2Te(11)	2.726(3)	Te(5)–Pd(3)–Te(13)	159.0(1)
Pd(3)–Te(13)	2.754(5)	Te(3)–Ta(3)–2Te(13)	84.42(8)
Pd(3)–Te(5)	2.811(5)	Te(4)–Ta(3)–2Te(3)	76.93(8)
Te(1)–Te(5)	3.125(4)	Te(4)–Ta(3)–2Te(13)	92.5(1)
Te(1)–2Te(14)	3.540(5)	Te(4)–Ta(3)–2Te(11)	86.38(9)
Te(2)–2Te(12)	3.375(4)	Te(3)–Ta(3)–Te(11)	157.5(1)
Te(2)–2Te(10)	3.492(5)	Te(13)–Ta(3)–2Te(11)	111.55(8)
Te(3)–Te(13)	3.514(5)	Te(1)–Ta(1)–2Te(5)	66.77(8)
Te(3)–2Te(3)	3.549(4)	Te(1)–Ta(1)–2Te(6)	147.20(9)
Te(3)–2Te(4)	3.685(6)	Te(9)–Ta(1)–Te(14)	125.1(2)
Te(4)–2Te(12)	3.651(5)	Te(1)–Ta(1)–2Te(9)	136.28(6)
Te(5)–2Te(9)	3.486(4)	Te(1)–Ta(1)–2Te(14)	75.90(9)
Te(14)–Ta(1)–2Te(5)	136.67(7)		
Te(14)–Ta(1)–2Te(6)	71.3(1)		
Te(9)–Ta(1)–2Te(5)	74.95(7)		
Te(9)–Ta(1)–2Te(6)	68.11(8)		
Te(5)–Ta(1)–2Te(6)	86.1(1)		
Te(8)–Ta(2)–2Te(10)	67.13(8)		
Te(8)–Ta(2)–2Te(12)	143.8(1)		
Te(7)–Ta(2)–Te(2)	127.7(1)		
Te(12)–Ta(2)–2Te(10)	87.86(8)		
Te(8)–Ta(2)–2Te(7)	74.25(8)		
Te(8)–Ta(2)–2Te(2)	136.35(7)		
Te(7)–Ta(2)–2Te(12)	69.61(8)		
Te(7)–Ta(2)–2Te(10)	136.17(6)		
Te(2)–Ta(2)–2Te(12)	71.7(1)		
Te(2)–Ta(2)–2Te(10)	74.44(9)		

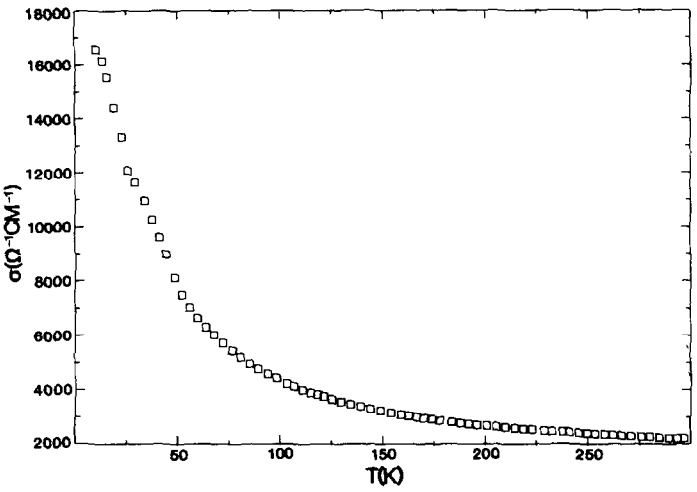

FIG. 7. Plot of conductivity vs temperature along b for $Ta_3Pd_3Te_{14}$: $\sigma_{297} \approx 2.2 \times 10^3\ \Omega^{-1}\ cm^{-1}$, $\sigma_{10} \approx 1.65 \times 10^4\ \Omega^{-1}\ cm^{-1}$.

vs temperature is given in Fig. 7. There is a large difference in the magnitude of the electrical conductivity of $Ta_3Pd_3Te_{14}$ and $TaNiTe_5$. We suspect that the substitution of Pd for Ni rather than the structural differences between the two compounds may be the primary cause of the difference in conductivity behavior.

It is interesting to compare the conductivity properties of $TaNiTe_5$ and $Ta_3Pd_3Te_{14}$ to some related tellurides. $TaTe_4$ (which has Ta in a square antiprismatic coordination (*38*)) exhibits linear metallic conductivity from 4.2 to 700 K (*39*). $ZrTe_3$ and $HfTe_3$, which possess chains of trigonal prismatically coordinated Zr and Hf, are metallic (*40*) and semiconducting (*41*), respectively. $ZrTe_5$ and $HfTe_5$, which also possess chains of trigonal prismatically coordinated Zr and Hf, are semimetals with a resistivity maximum at lower temperatures (*42*). Thus, the Group IV and Group V binary tellurides differ markedly in their conductivity properties. These properties offer no clues as to what to expect upon addition of a ternary element.

$Ta_3Pd_3Te_{14}$ is the first example where Ta occurs in two different coordination environments in a telluride compound, although mixed trigonal prismatic–octahedral coordination has been observed previously in the selenides, for example, in the compounds Ta_2NiSe_7 (*20*), Ta_2PtSe_7 (*20*), and $[Co_{1.5}Pt_{0.5}]Ta_6PtSe_{16}$ (*24*). $TaNiTe_5$ and $Ta_3Pd_3Te_{14}$ are the first examples of trigonal prismatic coordination of Ta in the tellurides. The usual coordination of Ta in tellurides is octahedral (*36*), square antiprismatic (*38*), or tetrahedral (*10*).

Nb and Ta have similar coordination preferences in the tellurides. Thus, it is not surprising that Ta has been substituted for Nb to yield the isostructural compounds $NbNiTe_5$ and $TaNiTe_5$. Ni and Pd also have similar coordination preferences in the tellurides. However, when a substitution of Pd for Ni is attempted, instead of preparing the expected isostructural compound $TaPdTe_5$, the compound $Ta_3Pd_3Te_{14}$ is prepared. Since Pt has the same coordination preferences as Ni or Pd it will be very interesting to see what effect the substitution of Pt for Pd or Ni has on stoichiometry, structure, and physical properties.

Acknowledgments

This research was supported by the U.S. National Science Foundation, Solid State Chemistry, Grant

DMR-83-15554 and in part by a NATO Research Grant 86-0438. This work made use of Central Facilities supported by the National Science Foundation through Northwestern University Materials Research Center, Grant DMR 85-20280. We are grateful for the use of the SQUID susceptometer in the Chemistry Department and the Center for Fundamental Materials Research at Michigan State University. We are indebted to Mr. Martin Godfrey for measuring the magnetic susceptibility of $TaNiTe_5$.

References

1. P. Haen, F. Lapierre, P. Monceau, M. Nuñez Regueiro, and J. Richard, *Solid State Commun.* **26,** 725 (1978).
2. J. A. Wilson, *Phys. Rev. B* **19,** 6456 (1979).
3. A. Meerschaut, L. Guemas, and J. Rouxel, *J. Solid State Chem.* **36,** 118 (1981).
4. M. S. Whittingham, *J. Solid State Chem.* **29,** 303 (1979).
5. R. R. Chianelli and M. B. Dines, *Inorg. Chem.* **14,** 2417 (1975).
6. J. Rouxel, *J. Solid State Chem.* **64,** 305 (1986).
7. G. Huan and M. Greenblatt, *Mater. Res. Bull.* **22,** 505 (1987).
8. G. Huan and M. Greenblatt, *Mater. Res. Bull.* **22,** 943 (1987).
9. P. Jensen and A. Kjekshus, *J. Less-Common Met.* **13,** 357 (1967).
10. F. Hulliger, *Helv. Phys. Acta* **34,** 379 (1961).
11. L. H. Brixner, Ger. DE 1185825 (1965).
12. E. W. Liimatta and J. A. Ibers, *J. Solid State Chem.* **71,** 384 (1987).
13. E. W. Liimatta and J. A. Ibers, submitted for publication.
14. E. Amberger, *Forschungsber. Bundesminist. Forsch. Technol. Technol. Forsch. Entwickl.*, BMFT-TB-T, 81-203 (1981).
15. D. A. Keszler and J. A. Ibers, *J. Solid State Chem.* **52,** 73 (1984).
16. D. A. Keszler, J. A. Ibers, M. Shang, and J. Lu, *J. Solid State Chem.* **57,** 68 (1985).
17. D. A. Keszler, P. J. Squattrito, N. E. Brese, J. A. Ibers, M. Shang, and J. Lu, *Inorg. Chem.* **24,** 3063 (1985).
18. D. A. Keszler and J. A. Ibers, *J. Amer. Chem. Soc.* **107,** 8119 (1985).
19. S. A. Sunshine and J. A. Ibers, *Inorg. Chem.* **24,** 3611 (1985).
20. S. A. Sunshine and J. A. Ibers, *Inorg. Chem.* **25,** 4355 (1986).
21. P. J. Squattrito, S. A. Sunshine, and J. A. Ibers, *Solid State Ionics* **22,** 53 (1986).
22. F. J. DiSalvo, C. H. Chen, R. M. Fleming, J. V. Waszczak, R. G. Dunn, S. A. Sunshine, and J. A. Ibers, *J. Less-Common Met.* **116,** 51 (1986).
23. P. J. Squattrito, S. A. Sunshine, and J. A. Ibers, *J. Solid State Chem.* **64,** 261 (1986).
24. S. A. Sunshine and J. A. Ibers, *J. Solid State Chem.* **69,** 219 (1987).
25. S. A. Sunshine and J. A. Ibers, *J. Solid State Chem.* **71,** 29 (1987).
26. S. A. Sunshine, D. A. Keszler, and J. A. Ibers, *Acc. Chem. Res.* **20,** 395 (1987).
27. MICROQ, Program from Tracorn Northern, Madison, WI.
28. T. E. Phillips, J. R. Anderson, C. J. Schramm, and B. M. Hoffman, *Rev. Sci. Instrum.* **50,** 263 (1979).
29. G. M. Sheldrick, *in* "Crystallographic Computing 3" (G. M. Sheldrick, C. Krugger, and R. Goddard, Eds.), pp. 175–189, Oxford Univ. Press, Oxford (1985).
30. J. M. Waters and J. A. Ibers, *Inorg. Chem.* **16,** 3273 (1977).
31. J. A. Ibers and W. C. Hamilton, Eds., "International Tables for X-ray Crystallography," Vol. IV, Tables 2.2A and 2.3.1, Kynoch Press, Birmingham (1974).
32. J. A. Ibers and W. C. Hamilton, *Acta Crystallogr.* **17,** 781 (1964).
33. R. D. Shannon, *Acta Crystallogr. Sect. A* **32,** 751 (1976).
34. L. N. Mulay and E. A. Boudreaux, Eds., "Theory and Application of Molecular Diamagnetism," Wiley–Interscience, New York (1976).
35. J. M. van den Berg and P. Cossee, *Inorg. Chim. Acta* **2,** 143 (1968).
36. B. E. Brown, *Acta Crystallogr.* **20,** 264 (1966).
37. S. Furuseth, K. Selte, and A. Kjekshus, *Acta Chem. Scand.* **19**(1), 257 (1965).
38. K. D. Bronsema, S. van Smaalen, J. L. De Boer, G. A. Wiegers, F. Jellinek, and J. Mahy, *Acta Crystallogr. Sect. B* **43,** 305 (1987).
39. J. Mahy, G. A. Wiegers, J. van Landuyt, and S. Amelinckx, *Mater. Res. Soc. Symp. Proc.* **21,** 181 (1984).
40. S. Takahashi, T. Sambongi, J. W. Brill, and W. Roark, *Solid State Commun.* **49**(11), 1031 (1984).
41. F. S. Khumalo and H. P. Hughes, *Phys. Rev. B* **22,** 2078 (1980).
42. F. J. DiSalvo, R. M. Fleming, and J. V. Waszczak, *Phys. Rev. B* **24,** 2935 (1981).
43. J. C. Huffman, Ph.D. Thesis, Indiana University (1974).
44. J. de Meulenaer and H. Tompa, *Acta Crystallogr.* **19,** 1014 (1965).
45. P. G. Lenhert, *J. Appl. Crystallogr.* **8,** 568 (1975).